

# Non-equilibrium dynamics of localization phase transition in the non-Hermitian Disorder-Aubry-André model

Yue-Mei Sun<sup>1,2</sup>, Xin-Yu Wang<sup>1,2</sup>, and Liang-Jun Zhai<sup>1,2\*</sup>

<sup>1</sup>The school of mathematics and physics, Jiangsu University of Technology, Changzhou 213001, China and

<sup>2</sup>The Jiangsu Key Laboratory of Clean Energy Storage and Conversion,  
Jiangsu University of Technology, Changzhou 213001, China

(Dated: November 20, 2024)

The driven dynamics of localization transitions in a non-Hermitian Disorder-Aubry-André (DAA) model are thoroughly examined under both open boundary conditions (OBC) and periodic boundary conditions (PBC). Through an analysis of the static properties of observables, including the localization length ( $\xi$ ), inverse participation ratio (IPR), and energy gap ( $\Delta E$ ), we found that the critical exponents examined under PBC are also applicable under OBC. The Kibble-Zurek scaling (KZS) for the driven dynamics in the non-Hermitian DAA systems is formulated and numerically verified for different quench directions. Notably, for the dynamical paths considered, boundary conditions had minimal impact on the evolution process. This study generalizes the application of the KZS to the dynamical localization transitions within systems featuring dual localization mechanisms.

## I. INTRODUCTION

The study of localization phase transition behaviors is a longstanding research topic in condensed matter physics [1–17]. Besides the Anderson model [1], the localization phase transition has also been found in the quasi-periodic systems, and various quasi-periodic models have been proposed, such as the Fibonacci model [18–20], the Aubry-André (AA) model and its various extensions [2, 21–29]. Studies have shown that there are certain differences in the localization phase transition between Anderson model and quasi-periodic models. For example, the localization phase transition can even occur for the one-dimensional (1D) AA model [2, 9, 10], and the critical exponents for the Anderson and AA models belong to two different universality classes [11, 30–33]. On the other hand, significant advancements in simulating nonequilibrium dynamics in quantum systems have been made [34–41]. Considerable attention has also been given to the nonequilibrium dynamics in localization transitions [42–45]. Several protocols have been employed to drive a quasi-periodic or disorder system out of equilibrium, such as suddenly changing the Hamiltonian [42, 46, 47], introducing a time-(quasi)periodic driving [48–50], or linearly quenching across the localization transition point [51–53]. Sudden quenching of the Anderson and AA models, with initial and post-quench Hamiltonians in different phases, will result in periodic zeros in the Loschmidt echo, indicating the localization-delocalization transition [42, 46]. The driven dynamics during a linear quench across the localization transition point can be accurately described by the Kibble-Zurek scaling (KZS) [51–53].

In recent years, the novel phenomena induced by non-Hermiticity have been extensively studied [54–64], including the non-Hermitian skin effect (NHSE) [65–68]

and exceptional points [69–73]. As discussions on non-Hermitian mechanisms have deepened, researchers have integrated these mechanisms into the study of localization [74–78]. The introduction of non-Hermiticity can give rise to a new dimension for tuning localization transitions and uncovers a series of exotic new phenomena [19, 74, 79–89]. For instance, the localization transition in the non-Hermitian quasi-periodic system is accompanied by a transition from real to complex eigenvalues, as well as a topological phase transition in the eigenvalue spectrum [24, 74, 79, 90]. And the NHSE suggests that changes in boundary conditions can result in substantial alterations in the bulk localization properties of non-Hermitian systems [75]. In addition, non-Hermiticity can also lead to critical exponents of the system belonging to different universality classes compared to the Hermitian case [55, 91].

Furthermore, the interplay between non-Hermiticity and non-equilibrium dynamics has also been studied [36–41, 49, 52, 91, 92]. For example, researchers studied the dynamical evolutions of the non-Hermitian AA model with a complex incommensurate lattice. They found that Loschmidt echo dynamics cannot detect dynamical phase transitions when the post-quench parameter is in the PT symmetry-broken regime [93]. Another example is that by applying Floquet time-periodic driving fields to non-Hermitian quasicrystals, one can dynamically control localization transitions and mobility edges as the field parameters vary [49]. Besides, studies have shown that the KZS remains valid in describing the driven dynamics of the non-Hermitian AA model under both open boundary conditions (OBC) [92] and periodic boundary conditions (PBC) [91].

More recently, researchers have increasingly focused on exploring the nonequilibrium dynamics of systems with multiple localization mechanisms [52, 53]. Bu et al. introduced a Disorder-Aubry-André (DAA) model, combining disorder and quasi-periodic localization, and investigated its driven dynamics [33, 52]. Their work proposed a new scaling mechanism, providing a novel perspective on the

---

\*Electronic address: [zhailiangjun@jsut.edu.cn](mailto:zhailiangjun@jsut.edu.cn)

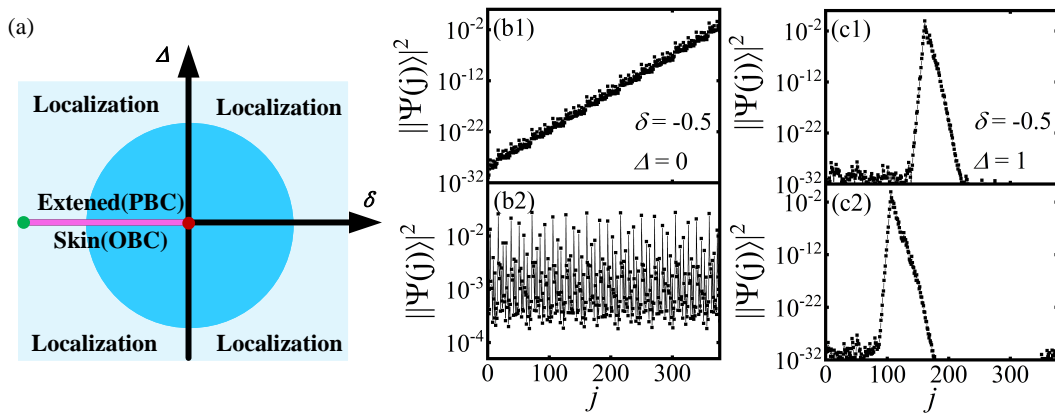


FIG. 1: (a) A schematic representation of the phase diagram for the non-Hermitian DAA model. When  $\delta = -2J_R$  (denoted by the green point), this model recovers the non-Hermitian Anderson model. The light blue region denotes the localization region, the blue region denotes the critical region, the red point denotes the critical point of the non-Hermitian DAA model. The purple line depicting the skin effect phase under OBC or the extended phase under PBC. The typical spatial distributions of the ground eigenstates for the non-Hermitian DAA model are shown for  $\Delta = 0$  under (b1) OBC and (b2) PBC. Similarly, the typical spatial distributions of the ground eigenstates for  $\Delta = 1$  are illustrated under (c1) OBC and (c2) PBC. In these simulations, we use  $g = 0.5$ ,  $\phi = 0$ ,  $\delta = -0.5$ , and  $L = 377$ .

study of localization phase transition dynamics in systems with coexisting multiple localization mechanisms. However, the interplay between the non-Hermiticity and the non-equilibrium dynamics in such systems remains unexplored. Here, we investigate the driven dynamics of localization transitions in a non-Hermitian DAA model with non-reciprocal hopping under both OBC and PBC. The KZS for the driven dynamics in the non-Hermitian DAA model is constructed and verified numerically across different quench directions. The rest of the paper is arranged as follows: the non-Hermitian DAA model and phase diagram are introduced in Sec. II. The static scaling properties are studied in Sec. III. Then, in Sec. IV, the KZS for the driven dynamics in the non-Hermitian DAA model under OBC and PBC is constructed and numerically verified. A summary is given in Sec. V.

## II. THE NON-HERMITIAN DAA MODEL AND PHASE DIAGRAM

The Hamiltonian of the non-Hermitian DAA model is defined by [94]

$$H = - \sum_j^L (J_L c_j^\dagger c_{j+1} + J_R c_{j+1}^\dagger c_j) + \Delta \sum_j^L w_j c_j^\dagger c_j (1) \\ + (2J_R + \delta) \sum_j^L \cos [2\pi(\gamma j + \phi)] c_j^\dagger c_j.$$

Here,  $c_j^\dagger(c_j)$  are creation (annihilation) operator of the hard-core boson and  $\gamma$  is an irrational number.  $J_L = Je^{-g}$  and  $J_R = Je^g$  are the asymmetry hopping coefficients.  $\Delta$  and  $(2J_R + \delta)$  measure the the amplitude

of disorder and the quasi-periodic potential, respectively.  $w_j \in [-1, 1]$  gives the quenched disorder configuration,  $\phi \in [0, 1)$  is phase of the potential. We assume  $J = 1$  as the unity of energy, and  $\gamma = (\sqrt{5} - 1)/2$ . To satisfy PBC of the quasi-periodic potential, we approximate  $\gamma$  as a rational number  $F_n/F_{n+1}$  where  $F_{n+1} = L$  and  $F_n$  are the Fibonacci numbers [74, 91].

A schematic phase diagram of the non-Hermitian DAA model near the critical point is illustrated in Fig. 1(a). For  $\delta = -2J_R$ , this model returns to the non-Hermitian Anderson model [2]. However, when  $\delta = 0$ , any finite  $\Delta$  can also cause localization at the critical point of the non-Hermitian AA model, but the localization characteristics in this case differ from those of the purely non-Hermitian Anderson model. Therefore, for the non-Hermitian DAA model, the point  $(\delta, \Delta) = (0, 0)$  represents its critical point, and the critical region surrounding this point is jointly defined by  $\Delta$  and  $\delta$ .

When  $\Delta = 0$ , this model recovers the non-Hermitian AA model [74]. For  $\delta > 0$ , all the eigenstates are localized under PBC and OBC. For  $\delta < 0$ , all the eigenstates are extended under PBC [91], whereas it exhibits the skin-effect phase under OBC [74, 92]. As illustrated in Figs. 1(b1) and (b2), the spatial distribution of the right eigenvector of the ground states ( $|\Psi(j)\rangle$ ) with  $\delta < 0$  and  $\Delta = 0$  under OBC and PBC are depicted, respectively. Here, the ground state is defined as the eigenstate possessing the smallest real eigenenergy among all possible states. It is shown that the wave function is localized on the boundary under OBC, but it is evenly distributed within a small range under PBC. For  $\delta > 0$ , the system will be in a localized state, regardless of the value of  $\Delta$ . For  $\delta < 0$ , any finite  $\Delta$  can also cause the system to transition into a localized state. As illustrated in Figs. 1(c1) and (c2), when  $\Delta = 1$  and  $\delta < 0$ , the spatial distribu-

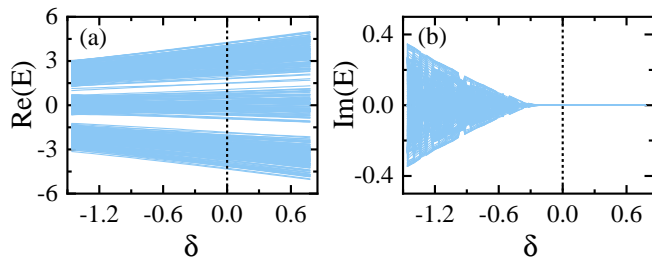


FIG. 2: (a) Real and (b) imaginary parts of energy spectra of the model Eq.(1) under OBC. The black dashed line corresponds to  $\delta = 0$ . Here, we choose  $g = 0.5$ ,  $\phi = 0.2$ ,  $\Delta = 0.8$  and  $L = 377$  in the calculation.

tion of localized states exhibits a high degree of similarity under both boundary conditions.

To discuss the impact of disorder on the localization phase transition in the non-Hermitian AA model, we further explore the energy spectrum of the non-Hermitian DAA model. Under PBC, the energy spectrum for the non-Hermitian AA model under PBC does not undergo significant changes when disorder is introduced, but it disrupts the correspondence between the transition from real to complex of energy spectrum and the localization transition [94]. Here, Fig. 2 displays the energy spectrum of the non-Hermitian DAA model under OBC. The results show that, unlike the fully real energy spectrum of the non-Hermitian AA model under OBC [74], the introduction of disorder leads to the emergence of imaginary parts in the energy spectrum in the region where  $\delta < 0$ .

### III. STATIC CRITICAL PROPERTIES OF THE NON-HERMITIAN DAA MODEL

#### A. Static scaling forms in the critical region

In this section, we study the static properties within the critical region, utilizing the localization length ( $\xi$ ), the inverse participation ratio (IPR), and the energy gap between the ground state and the first excited state ( $\Delta E$ ).

As in the usual quantum criticality, the localization length  $\xi$  for the non-Hermitian system is given by [51, 91]

$$\xi = \sqrt{\sum_{n>n_c}^L [(n - n_c)^2] P_i}, \quad (2)$$

where  $P_i$  denotes the probability of the wavefunction at site  $i$ , and  $n_c \equiv \sum n P_i$  represents the localization center. In the vicinity of a critical point,  $\xi$  scales with the distance to the critical point  $\varepsilon$  as [2]

$$\xi \propto \varepsilon^{-\nu}, \quad (3)$$

where  $\nu$  is a critical exponent. For the pure non-Hermitian AA model, under both PBC and OBC,  $\varepsilon = \delta$

and  $\nu = \nu_\delta = 1$  [91, 92]. For the pure non-Hermitian Anderson model,  $\varepsilon = \Delta$  and  $\nu = \nu_A = 1.99$  [94]. For the non-Hermitian DAA model,  $\Delta$  constitutes another significant factor at  $(\delta, \Delta) = (0, 0)$  [33, 94]. Specifically, when  $\delta = 0$  in Eq. (1),  $\varepsilon = \Delta$  and  $\nu = \nu_\Delta = 0.52$  under PBC [94].  $\nu_\Delta$  is a new parameter distinct from that of the non-Hermitian Anderson model and the non-Hermitian AA model.

The IPR is defined as [95, 96]

$$\text{IPR} = \frac{\sum_{j=1}^L |\Psi(j)|^4}{\sum_{j=1}^L |\Psi(j)|^2}. \quad (4)$$

In the extended states, the scaling of IPR is given by  $\text{IPR} \propto L^{-1}$ . For the localized states or skin effect states, the scaling is  $\text{IPR} \propto L^0$  [74]. At the critical point, the IPR scales as

$$\text{IPR} \propto L^{-s/\nu}, \quad (5)$$

where  $s$  is a critical exponent. As  $L$  approaches infinity, the IPR scales with the distance to the critical point  $\varepsilon$  according to

$$\text{IPR} \propto \varepsilon^s. \quad (6)$$

For the non-Hermitian AA model, under both OBC and PBC, it is found that  $\varepsilon = \delta$  and  $s = s_\delta = 0.1197$  [19, 91].

At the critical point of localization transition, the energy gap  $\Delta E$  exhibits a scaling relationship with the lattice size  $L$ , given by

$$\Delta E \propto L^{-z}, \quad (7)$$

where  $z$  is a critical exponent. For the non-Hermitian AA model, under both OBC and PBC, it is found that  $\varepsilon = \delta$  and  $z = z_\delta = 2$  [91]. when  $L$  tends to infinity, energy gap  $\Delta E$  scales as

$$\Delta E \propto \varepsilon^{\nu z}. \quad (8)$$

Considering the finite-size effect, the general scaling formulation for a quantity  $Y$  referring to a single parameter can be expressed as:

$$Y(\varepsilon) = L^{y/\nu} f(\varepsilon L^{1/\nu}), \quad (9)$$

where  $y$  is the critical exponent of  $Y$ , defined such that  $Y \propto \varepsilon^{-y}$  as  $L \rightarrow \infty$ . The function  $f(\cdot)$  represents the scaling function. By taking  $\Delta$  and  $\delta$  as scaling variables simultaneously, the comprehensive finite-size scaling expressions for the three observables are given by

$$\xi = L f_1(\delta L^{1/\nu_\delta}, \Delta L^{1/\nu_\Delta}), \quad (10)$$

$$\text{IPR} = L^{-s_\delta/\nu_\delta} f_2(\delta L^{1/\nu_\delta}, \Delta L^{1/\nu_\Delta}), \quad (11)$$

$$\Delta E = L^{-z_\delta} f_3(\delta L^{1/\nu_\delta}, \Delta L^{1/\nu_\Delta}). \quad (12)$$

These scaling functions, Eqs. (10) to (12), are applicable within the critical region of the non-Hermitian DAA model.

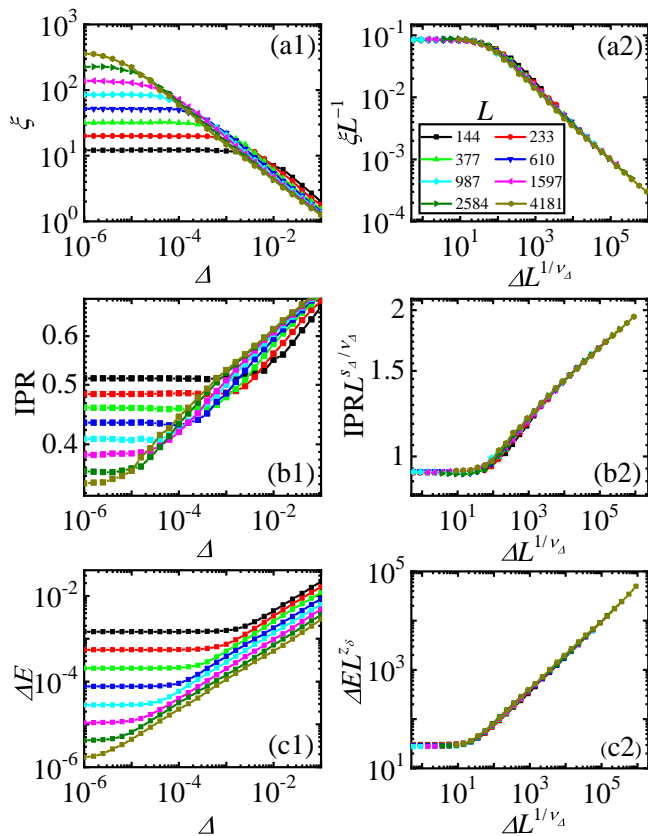


FIG. 3: Scaling properties in the ground state for fixed  $\delta L^{1/\nu_\delta} = 1$  under OBC. The curves of  $\xi$  versus  $\Delta$  before (a1) and after (a2) rescaled for different  $L$ 's. The curves of IPR versus  $\Delta$  before (b1) and after (b2) rescaled for different  $L$ 's. The curves of  $\Delta E$  versus  $\Delta$  before (c1) and after (c2) rescaled for different  $L$ 's. Here,  $g = 0.5$ , and the result is averaged for 1000 samples. The double-logarithmic scales are used.

## B. Numerical results of static scaling of the non-Hermitian DAA model

The critical exponents of the non-Hermitian DAA model under PBC have been examined [94]. It is found that the critical exponents vary along the  $\delta$  and  $\Delta$  directions because these parameters represent two distinct relevant directions. Under PBC, the critical exponents along  $\delta$  direction with  $\Delta = 0$  are  $(\nu, s, z) = (\nu_\delta, s_\delta, z_\delta) = (1, 0.1197, 2)$  [91]. In contrast, the scaling exponents along the  $\Delta$  direction are  $(\nu, s, z) = (\nu_\Delta, s_\Delta, z_\Delta) = (0.52, 0.0642, 2)$ .

Here, we study the static scaling properties of the non-Hermitian DAA model under OBC by employing the exponents obtained from fitting under PBC. We numerically validate Eqs. (10) to (12) under OBC by maintaining  $\delta L^{1/\nu_\delta}$  at a constant value. Fig. 3 depict the scaling behavior of  $\xi$ , IPR and  $\Delta E$  as functions of  $\Delta$  for  $\delta L^{1/\nu_\delta} = 1$ . After rescaling these values according to Eqs. (10) to (12), the resulting curves align closely, thereby confirming the validity of these equations. For the critical region where  $\delta < 0$ , similar numerical results

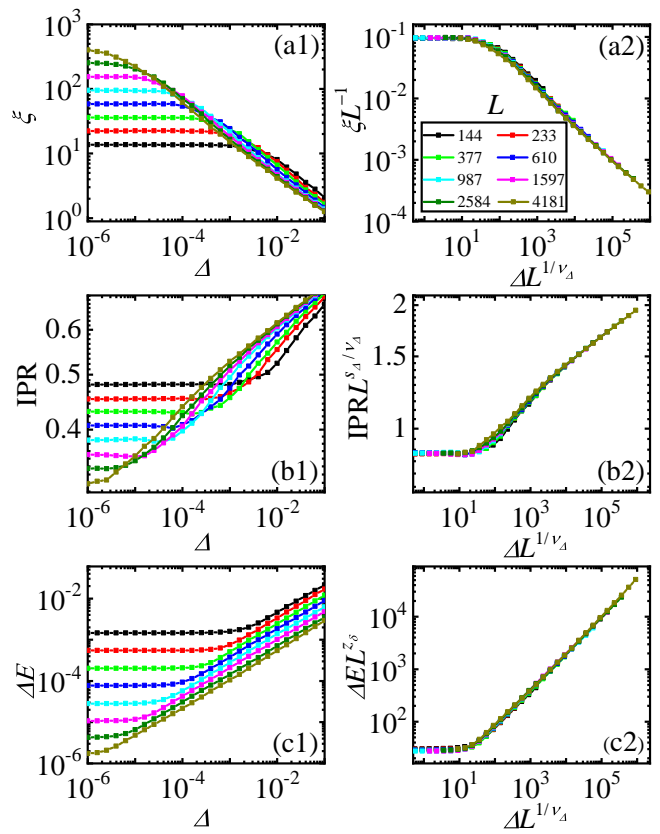


FIG. 4: Scaling properties in the ground state for fixed  $\delta L^{1/\nu_\delta} = -1$  under OBC. The curves of  $\xi$  versus  $\Delta$  before (a1) and after (a2) rescaled for different  $L$ 's. The curves of IPR versus  $\Delta$  before (b1) and after (b2) rescaled for different  $L$ 's. The curves of  $\Delta E$  versus  $\Delta$  before (c1) and after (c2) rescaled for different  $L$ 's. Here,  $g = 0.5$ , and the result is averaged for 1000 samples. The double-logarithmic scales are used.

are presented in Fig. 4 for  $\delta L^{1/\nu_\delta} = -1$ . The alignment of the rescaled curves shown in Figs. 4 (a2), (b2) and (c2) further verifies Eqs. (10) to (12).

These results confirm that the same set critical exponent of the non-Hermitian DAA model under PBC is typically sufficient to characterize the critical behavior in the critical region under OBC.

## IV. KZS FOR THE DRIVEN DYNAMICS OF THE NON-HERMITIAN DAA MODEL

### A. General theory of the KZS

We proceed to investigate the KZS associated with the driven dynamics within the non-Hermitian DAA model. Our analysis assumes that the system begins in a localized state and is subsequently driven through the critical region by linearly adjusting the distance  $\varepsilon$  over time  $t$  with a constant rate  $R$ . The temporal evolution of  $\varepsilon$  is

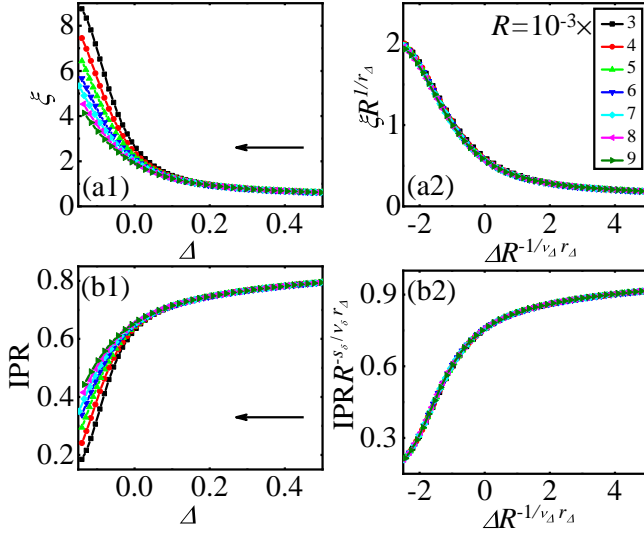


FIG. 5: KZS of driven dynamics in the non-Hermitian DAA model with fixed  $\delta = 0$  under OBC. Curves of  $\xi$  versus  $\Delta$  before (a1) and after (a2) rescaling for different driving rates  $R$ . Curves of IPR versus  $\Delta$  before (b1) and after (b2) rescaling for different  $R$ . The lattice size is  $L = 610$ ,  $\phi = 0$ ,  $g = 0.5$  and one sample of  $w_j$  is used.

described by

$$\varepsilon = \varepsilon_0 - Rt, \quad (13)$$

where  $\varepsilon$  can represent either  $\Delta$  or  $\delta$ , depending on the specific situation being analyzed,  $\varepsilon_0 > 0$  denotes the initial distance from the critical point at  $t = 0$ . According to the KZS, if  $|\varepsilon| > R^{1/r\nu}$  with the scaling exponent  $r = z + 1/\nu$ , the system has enough time to adapt to changes in the Hamiltonian, maintaining adiabatic conditions. Conversely, when  $|\varepsilon| < R^{1/r\nu}$ , the system's internal change rate lags behind the external parameter's rate, indicating the system entry into the impulse region [97–99]. Below, we choose the system size  $L = 610$ , which is sufficiently large to disregard finite-size effects in realtime simulations. We initialize the system in its ground state with a fixed  $\varepsilon_0$  value of 1.0.

Apparently, there are two adjustable variables  $\Delta$  and  $\delta$  in the non-Hermitian DAA model. Thus, both of these relevant terms should be incorporated into the full KZS form. The evolution of the localization length  $\xi$  should satisfy [52, 53]

$$\xi(\Delta, \delta, R) = R^{-\frac{1}{r_\Delta}} f_4(\delta R^{-\frac{1}{r_\Delta \nu_\delta}}, \Delta R^{-\frac{1}{r_\Delta \nu_\Delta}}), \quad (14)$$

where  $r_\Delta = z_\Delta + 1/\nu_\Delta$ . Similarly, IPR should satisfy

$$\text{IPR}(\Delta, \delta, R) = R^{\frac{s_\delta}{r_\Delta \nu_\delta}} f_5(\delta R^{-\frac{1}{r_\Delta \nu_\delta}}, \Delta R^{-\frac{1}{r_\Delta \nu_\Delta}}). \quad (15)$$

Eq. (14) and Eq. (15) should be applicable for a range of  $\Delta$  and  $\delta$  values in proximity to the critical region of the non-Hermitian DAA model.

In order to verify the KZS, we can either set some variables to zero or fix the values of certain variables.

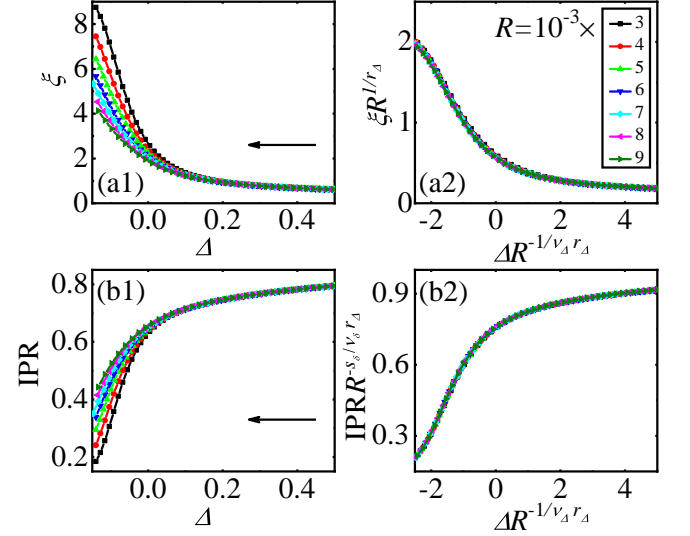


FIG. 6: KZS of driven dynamics in the non-Hermitian DAA model with fixed  $\delta = 0$  under PBC. Curves of  $\xi$  versus  $\Delta$  before (a1) and after (a2) rescaling for different driving rates  $R$ . Curves of IPR versus  $\Delta$  before (b1) and after (b2) rescaling for different  $R$ . The lattice size is  $L = 610$ ,  $\phi = 0$ ,  $g = 0.5$  and one sample of  $w_j$  is used.

When  $\Delta = 0$ , the model (1) corresponds to the non-Hermitian AA model, and the KZS for the non-Hermitian AA model have been validated [91, 92]. When  $\delta = 0$ , Eq. (14) and Eq. (15) return to

$$\xi(\Delta, R) = R^{-1/r_\Delta} f_6(\Delta R^{-1/r_\Delta \nu_\Delta}), \quad (16)$$

$$\text{IPR}(\Delta, R) = R^{s_\delta/r_\Delta \nu_\delta} f_7(\Delta R^{-1/r_\Delta \nu_\Delta}). \quad (17)$$

This corresponds to the situation where a dynamic quench of the system is conducted along the direction of  $\Delta$ , with  $\delta$  fixed at 0. For the case where  $\delta \neq 0$ , we can also fix  $\delta R^{-1/r_\Delta \nu_\delta}$ , and  $\Delta R^{-1/r_\Delta \nu_\Delta}$  to verify Eq. (14) and Eq. (15).

## B. Numerical results of driven dynamics

First, we verify the scaling function Eq. (16) and Eq. (17) with the initial state deep in the localization state by linearly varying the value of the disorder potential  $\Delta$ . The numerical results for  $\xi$  and IPR as functions of  $\Delta$  for various driving rates  $R$  under OBC are depicted in Fig. 5(a1) and Fig. 5(b1), respectively. Observation reveals that the curves corresponding to different  $R$  diverge from each other near the critical region. However, when these curves are rescaled using the critical exponents of the non-Hermitian DAA model, they converge near the critical region, as illustrated in Fig. 5(a2) and Fig. 5(b2). This convergence aligns with the predictions of Eq. (16) and Eq. (17). Additionally, in Fig. 6, the dynamics of  $\xi$  and IPR under PBC are plotted. Similarly, the rescaled curves collapse onto each other, confirming Eq. (16) and Eq. (17).

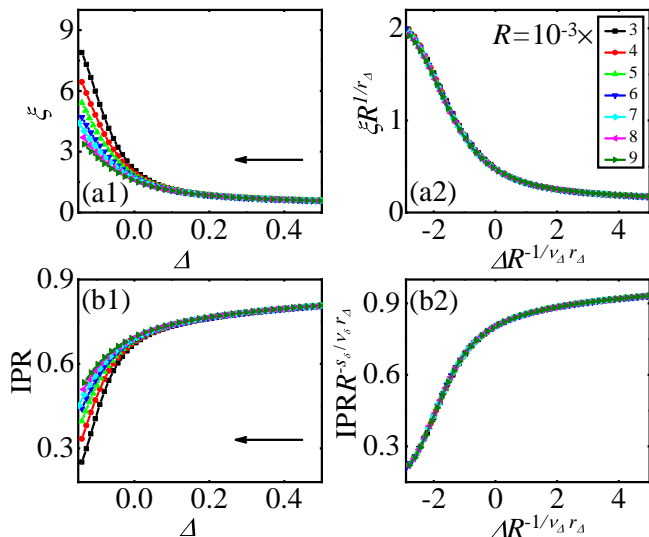


FIG. 7: KZS of driven dynamics in the non-Hermitian DAA model with fixed  $\delta R^{-1/r_{\Delta}\nu_{\delta}} = 0.3$  under OBC. Curves of  $\xi$  versus  $\Delta$  before (a1) and after (a2) rescaling for different driving rates  $R$ . Curves of IPR versus  $\Delta$  before (b1) and after (b2) rescaling for different  $R$ . The lattice size is  $L = 610$ ,  $\phi = 0$ ,  $g = 0.5$  and one sample of  $w_j$  is used.

Then, we verify the KZS forms of  $\xi$  and IPR by fixing  $\delta R^{-1/r_{\Delta}\nu_{\delta}} = 0.3$ , which is demonstrated in Fig. 7. We numerically compute the time evolutions of  $\xi$  and IPR for various driving rate  $R$  under OBC, with results presented in Fig. 7(a1) and Fig. 7(b1), respectively. Upon rescaling the quantities according to Eq. (14) and Eq. (15), we observe that the curves corresponding to different  $R$  converge near the critical region in Fig. 7(a2) and Fig. 7(b2). Similar results for  $\xi$  and IPR under PBC are plotted in Fig. 8. After rescaling with  $R$ , the rescaled curves align with each other as shown in Fig. 8(a2) and Fig. 8(b2), confirming Eq. (14) and Eq. (15). We have also numerically verified the KZS for the non-Hermitian DAA model by linearly varying the value of the quasiperiodic potential  $\delta$ . By fixing  $\Delta R^{-1/r_{\Delta}\nu_{\Delta}} = 0.3$ , we calculate the evolution of  $\xi$  and IPR for various driving rates  $R$ , starting from the initial state. By rescaling these evolution curves with respect to  $R$ , we observe that the rescaled curves align with each other, as illustrated in Fig. 9, confirming Eq. (14) and Eq. (15). In Fig. 10, we present the evolution of  $\xi$  and IPR under PBC. After rescaling the curves converge onto one another, in accordance with Eq. (14) and Eq. (15). These findings demonstrate the validity of the KZS in both  $\Delta$  and  $\delta$  directions near the critical region of the non-Hermitian DAA model.

Furthermore, we also observe that for each of the three quenching paths we considered, there is basically no difference in the results of the dynamic numerical simulations between OBC and PBC. This phenomenon can be understood from the following two aspects. Firstly, all three dynamic evolution processes involve transitions from a localized state, passing through a critical region, and ending up in another localized state. The localized

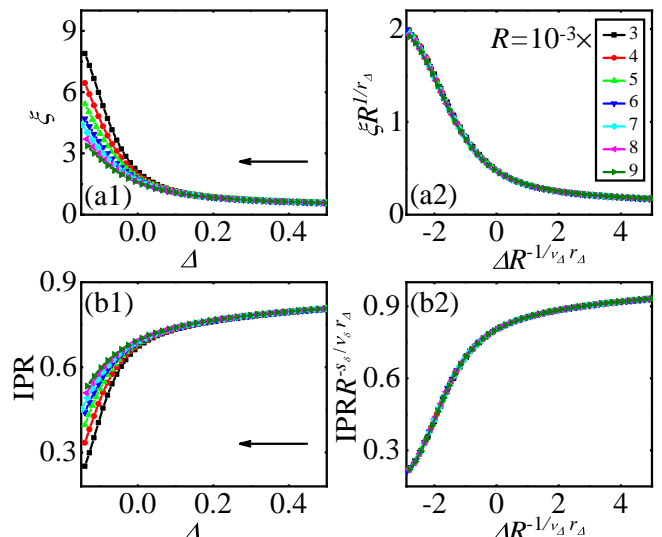


FIG. 8: KZS of driven dynamics in the non-Hermitian DAA model with fixed  $\delta R^{-1/r_{\Delta}\nu_{\delta}} = 0.3$  under PBC. Curves of  $\xi$  versus  $\Delta$  before (a1) and after (a2) rescaling for different driving rates  $R$ . Curves of IPR versus  $\Delta$  before (b1) and after (b2) rescaling for different  $R$ . The lattice size is  $L = 610$ ,  $\phi = 0$ ,  $g = 0.5$  and one sample of  $w_j$  is used.

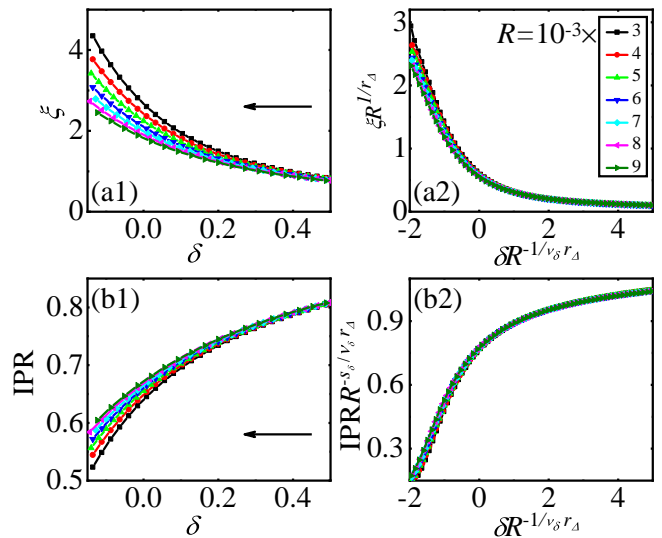


FIG. 9: KZS of driven dynamics in the non-Hermitian DAA model with fixed  $\Delta R^{-1/r_{\Delta}\nu_{\Delta}} = 0.3$  under OBC. Curves of  $\xi$  versus  $\delta$  before (a1) and after (a2) rescaling for different driving rates  $R$ . Curves of IPR versus  $\delta$  before (b1) and after (b2) rescaling for different  $R$ . The lattice size is  $L = 610$ ,  $\phi = 0$ ,  $g = 0.5$  and one sample of  $w_j$  is used.

states are not sensitive to changes in boundary conditions between OBC and PBC. Secondly, for each of the three paths we considered, their energy spectra exhibit similar characteristics under both OBC and PBC. For the case where  $\delta = 0$  and  $\Delta$  is varied, the energy spectra under both OBC and PBC are basically no difference; for the case where  $\delta R^{-1/r_{\Delta}\nu_{\delta}}$  is fixed and  $\Delta$  is varied, the energy spectra under both OBC and PBC are real; for the case

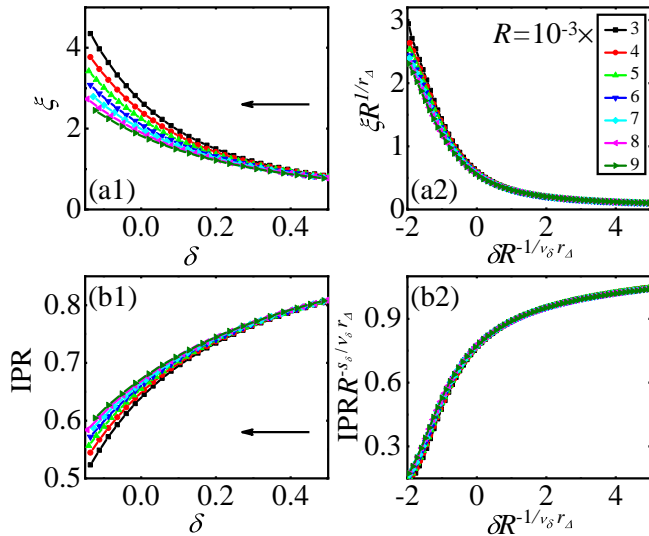


FIG. 10: KZS of driven dynamics in the non-Hermitian DAA model with fixed  $\Delta R^{-1/r_{\Delta\nu\Delta}} = 0.3$  under PBC. Curves of  $\xi$  versus  $\delta$  before (a1) and after (a2) rescaling for different driving rates  $R$ . Curves of IPR versus  $\delta$  before (b1) and after (b2) rescaling for different  $R$ . The lattice size is  $L = 610$ ,  $\phi = 0$ ,  $g = 0.5$  and one sample of  $w_j$  is used.

where  $\Delta R^{-1/r_{\Delta\nu\Delta}}$  is fixed and  $\delta$  is varied, the energy spectrum undergoes a transition from real to imaginary under both OBC and PBC.

## V. SUMMARY

In summary, we have conducted a comprehensive study of the static scaling behavior and the driven dynamics of localization transitions in the non-Hermitian DAA

model, considering both OBC and PBC. By examining the static behavior of  $\xi$ , IPR and  $\Delta E$ , we have demonstrated that the same critical exponents observed under PBC are also valid under OBC. We constructed the KZS for driven dynamics of the non-Hermitian DAA systems and numerically confirmed its validity across three different quench directions. For the dynamical paths we considered, the boundary conditions do not have a significant impact on the dynamical evolution process. Our work generalizes the application of the KZS to the dynamical localization transitions within systems featuring dual localization mechanisms.

On-site gain and loss constitute another crucial aspect of non-Hermiticity [100, 101], with numerous studies highlighting its distinct influence on localization compared to nonreciprocal effects. Hence, investigating the non-Hermitian DAA model that incorporates on-site gain and loss stands as a potential and fruitful extension of this paper. Additionally, the absence of a mobility edge in the excited states of DAA model has been demonstrated [33, 94]. However, the introduction of dynamic driving to systems that do possess a mobility edge may result in unique phenomena, necessitating further exploration and discussion.

## Acknowledgments

This work is supported by the National Natural Science Foundation of China (Grant No. 12274184), the Qing Lan Project, the National Natural Science Foundation of China (Grant No. 12404105) and the Natural Science Foundation of the Jiangsu Higher Education Institutions of China (Grant No. 24KJB140008).

- 
- [1] P. W. Anderson, Absence of diffusion in certain random lattices, *Phys. Rev.* **109**, 1492 (1958).
  - [2] S. Aubry and G. André, Analyticity breaking and anderson localization in incommensurate lattices, *Ann. Israel Phys. Soc.* **3**, 133 (1980).
  - [3] J. Biddle and S. Das Sarma, Predicted mobility edges in one-dimensional incommensurate optical lattices: An exactly solvable model of anderson localization, *Phys. Rev. Lett.* **104**, 070601 (2010).
  - [4] S. Xu, X. Li, Y.-T. Hsu, B. Swingle, and S. Das Sarma, Battered effect in interacting Aubry-André model: Thermalization, slow scrambling, and many-body localization, *Phys. Rev. Research* **1**, 032039 (2019).
  - [5] V. Khemani, D. N. Sheng, and D. A. Huse, Two universality classes for the many-body localization transition, *Phys. Rev. Lett.* **119**, 075702 (2017).
  - [6] H. Yao, A. Khoudli, L. Bresque, and L. Sanchez-Palencia, Critical behavior and fractality in shallow one-dimensional quasiperiodic potentials, *Phys. Rev. Lett.* **123**, 070405 (2019).
  - [7] J. Schirmann, S. Franca, F. Flicker, and A. G. Grushin, Physical Properties of an Aperiodic Monotile with Graphene-like Features, Chirality, and Zero Modes, *Phys. Rev. Lett.* **132**, 086402 (2024).
  - [8] M. Gonçalves, B. Amorim, E. V. Castro, and P. Ribeiro, Critical Phase Dualities in 1D Exactly Solvable Quasiperiodic Models, *Phys. Rev. Lett.* **131**, 186303 (2024).
  - [9] J. Šuntajs, T. c. v. Prosen, and L. Vidmar, Localization challenges quantum chaos in the finite two-dimensional Anderson model, *Phys. Rev. B* **107**, 064205 (2023).
  - [10] A. Yamilov, S. E. Skipetrov, T. W. Hughes, M. Minkov, Z. Yu, and H. Cao, Anderson localization of electromagnetic waves in three dimensions, *Nat. Phys.* **19**, 1308 (2023).
  - [11] U. Agrawal, S. Gopalakrishnan, and R. Vasseur, Universality and quantum criticality in quasiperiodic spin chains, *Nat. Commun.* **11**, 2225 (2020).
  - [12] U. Agrawal, S. Gopalakrishnan, and R. Vasseur, Quantum Criticality in the 2D Quasiperiodic Potts Model, *Phys. Rev. Lett.* **125**, 265702 (2020).
  - [13] V. Goblot, A. Štrkalj, N. Pernet, J. L. Lado, C. Dorow,

- A. Lemaître, L. L. Gratiet, A. Harouri, I. Sagnes, S. Ravets, A. Amo, J. Bloch, and O. Zilberberg, Emergence of criticality through a cascade of delocalization transitions in quasiperiodic chains, *Nat. Phys.* **16**, 832 (2020).
- [14] S. Roy, S. Chattopadhyay, T. Mishra, and S. Basu, Critical analysis of the reentrant localization transition in a one-dimensional dimerized quasiperiodic lattice, *Phys. Rev. B* **105**, 214203 (2022).
- [15] U. Agrawal, R. Vasseur, and S. Gopalakrishnan, Quasiperiodic many-body localization transition in dimension  $d > 1$ , *Phys. Rev. B* **106**, 094206 (2022).
- [16] X.-C. Zhou, Y.-J. Wang, T.-F. J. Poon, Q. Zhou, and X.-J. Liu, Exact New Mobility Edges between Critical and Localized States, *Phys. Rev. Lett.* **131**, 176401 (2023).
- [17] A. Smith, J. Knolle, R. Moessner, D. L. Kovrizhin, Absence of ergodicity without quenched disorder: From quantum disentangled liquids to many-body localization, *Phys. Rev. Lett.* **119**, 176601 (2017).
- [18] A. Štrkalj, E. V. H. Doggen, I. V. Gornyi, and O. Zilberberg, Many-body localization in the interpolating Aubry-André-Fibonacci model, *Phys. Rev. Research* **3**, 033257 (2021).
- [19] L.-J. Zhai, G.-Y. Huang, and S. Yin, Cascade of the delocalization transition in a non-Hermitian interpolating Aubry-André-Fibonacci chain, *Phys. Rev. B* **104**, 014202 (2021).
- [20] C. Y. Guo, Multiple intermediate phases in the interpolating Aubry-André-Fibonacci model, *Phys. Rev. B* **109**, 174203 (2024).
- [21] S. Das Sarma, S. He, and X. C. Xie, Mobility Edge in a Model One-Dimensional Potential, *Phys. Rev. Lett.* **61**, 2144 (1988).
- [22] J. Biddle, D. J. Priour, B. Wang, and S. Das Sarma, Localization in one-dimensional lattices with non-nearest-neighbor hopping: Generalized Anderson and Aubry-André models, *Phys. Rev. B* **83**, 075105 (2011).
- [23] Y. Wang, X. Xia, L. Zhang, H. Yao, S. Chen, J. You, Q. Zhou, and X.-J. Liu, One-dimensional quasiperiodic mosaic lattice with exact mobility edges, *Phys. Rev. Lett.* **125**, 196604 (2020).
- [24] Y. Liu, Y. Wang, X.-J. Liu, Q. Zhou, and S. Chen, Exact mobility edges, PT-symmetry breaking, and skin effect in one-dimensional non-hermitian quasicrystals, *Phys. Rev. B* **103**, 014203 (2021).
- [25] J. Gao, Ivan M. Khaymovich, X.-W. Wang, Z.-S. Xu, A. Iovan, G. Krishna, J. Jiensi, A. Cataldo, A. V. Balatsky, V. Zwiller, and A. W. Elshaari, Probing multimobility edges in quasiperiodic mosaic lattices, *Sci. Bull.* **09**, 030 (2024).
- [26] T. Lv, Y.-B. Liu, T.-C. Yi, L. Li, M. Liu, and W.-L. You, Exploring unconventional quantum criticality in the  $p$ -wave-paired Aubry-André-Harper model, *Phys. Rev. B* **106**, 144205 (2022).
- [27] S. Longhi, Metal-insulator phase transition in a non-Hermitian Aubry-André-Harper model, *Phys. Rev. B* **100**, 125157 (2019).
- [28] C.-C. Zeng, Z. Cai, G.-H. Wang, and G. Sun, Fidelity and criticality in the nonreciprocal Aubry-André-Harper model, arXiv:2404.16704 (2024).
- [29] Y. Wang, C. Cheng, X.-J. Liu, and D. Yu, Many-Body Critical Phase: Extended and Nonthermal, *Phys. Rev. Lett.* **126**, 080602 (2021).
- [30] B.-B. Wei, Fidelity susceptibility in one-dimensional disordered lattice models, *Phys. Rev. A* **99**, 042117 (2019).
- [31] T. Wang, T. Ohtsuki, and R. Shindou, Universality classes of the Anderson transition in the three-dimensional symmetry classes AIII, BDI, C, D, and CI, *Phys. Rev. B* **104**, 014206 (2021).
- [32] J. C. C. Cestari, A. Foerster, M. A. Gusmão, and M. Continentino, Critical exponents of the disorder driven superfluid-insulator transition in one-dimensional Bose-Einstein condensates, *Phys. Rev. A* **84**, 055601 (2011).
- [33] X. Bu, L.-J. Zhai, and S. Yin, Quantum criticality in the disordered Aubry-André model, *Phys. Rev. B* **106**, 214208 (2022).
- [34] X. H. Wang and J. Wang, Mpemba effects in nonequilibrium open quantum systems, *Phys. Rev. Research* **6**, 033330 (2024).
- [35] J. J. Chen and K. Dorfman, Entangled two-photon quantum heat engine: Dissipative nonequilibrium dynamics and correlated statistics, *Phys. Rev. Research* **6**, 023237 (2024).
- [36] J.-Q. Cheng, S. Yin, and D.-X. Yao, Dynamical localization transition in the non-Hermitian lattice gauge theory, *Commun. Phys.* **7**, 58 (2024).
- [37] H. X. Gao, K. K. Wang, L. Xiao, M. Nakagawa, N. Matsumoto, D. K. Qu, H. Q. Lin, M. Ueda, and P. Xue, Experimental Observation of the Yang-Lee Quantum Criticality in Open Quantum Systems, *Phys. Rev. Lett.* **132**, 1776601 (2024).
- [38] K. Zhang, C. Fang, and Z. S. Yang, Dynamical Degeneracy Splitting and Directional Invisibility in Non-Hermitian Systems, *Phys. Rev. Lett.* **131**, 036402 (2023).
- [39] L.-T. You, Y.-J. Gao, G.-T. Wang, and G.-P. Zheng, Chiral dynamics of three-mode non-Hermitian systems with a periodical driving, *Phys. Rev. A* **109**, 062218 (2024).
- [40] J. Mák, M. J. Bhaseen and A. Pal, Statics and dynamics of non-Hermitian many-body localization, *Commun. Phys.* **7**, 92 (2024).
- [41] Z. Li, L.-W. Wang, X. L. Wang, Z.-K. Lin, G. C. Ma, and J.-H. Jiang, Observation of dynamic non-Hermitian skin effects, *Nat. Commun.* **15**, 6544 (2024).
- [42] C. Yang, Y. C. Wang, P. Wang, X. L. Gao, and S. Chen, Dynamical signature of localization-delocalization transition in a one-dimensional incommensurate lattice, *Phys. Rev. B* **95**, 184201 (2017).
- [43] M. Heyl, Dynamical quantum phase transitions: a review, *Rep. Prog. Phys.* **81**, 054001 (2018).
- [44] B. Bertini, P. Kos, and T. Prosen, Localized Dynamics in the Floquet Quantum East Model, *Phys. Rev. Lett.* **132**, 080401 (2024).
- [45] A. Khan, W. Chen, M. Jan, G. Xianlong, Linear-scale simulations of quench dynamics, *Comput. Phys. Commun.* **132**, 109132 (2024).
- [46] H. H. Yin, S. Chen, X. L. Gao, and P. Wang, Zeros of Loschmidt echo in the presence of Anderson localization, *Phys. Rev. A* **97**, 033624 (2018).
- [47] R. Modak and D. Rakshit, Many-body dynamical phase transition in a quasiperiodic potential, *Phys. Rev. B* **103**, 224310 (2021).
- [48] K. Yang, L. Zhou, W. Ma, X. Kong, P. Wang, X. Qin, X. Rong, Y. Wang, F. Shi, J. Gong, and J. Du, Floquet dynamical quantum phase transitions, *Phys. Rev.*



- B **100**, 085308 (2019).
- [49] L. W. Zhou, Floquet engineering of topological localization transitions and mobility edges in one-dimensional non-Hermitian quasicrystals, *Phys. Rev. Research* **3**, 033184 (2021).
- [50] L. W. Zhou and Q. Q. Du, Floquet dynamical quantum phase transitions in periodically quenched systems, *J. Phys.: Condens. Matter* **33**, 345403 (2021).
- [51] A. Sinha, M. M. Rams, and J. Dziarmaga, Kibble-zurek mechanism with a single particle: Dynamics of the localization-delocalization transition in the Aubry-André model, *Phys. Rev. B* **99**, 094203 (2019).
- [52] X. Bu, L.-J. Zhai, and S. Yin, Kibble-Zurek scaling in one-dimensional localization transitions, *Phys. Rev. A* **108**, 023312 (2023).
- [53] E.-W. Liang, L.-Z. Tang, and D.-W. Zhang, Quantum criticality and Kibble-Zurek scaling in the Aubry-André-Stark model, *Phys. Rev. B* **110**, 024207 (2024).
- [54] S. Longhi, Topological phase transition in non-Hermitian quasicrystals, *Phys. Rev. Lett.* **122**, 237601 (2019).
- [55] X. Luo, T. Ohtsuki, and R. Shindou, Universality Classes of the Anderson Transitions Driven by Non-Hermitian Disorder, *Phys. Rev. Lett.* **126**, 090402 (2021).
- [56] Y. C. Jing, J.-J. Dong, Y.-Y. Zhang, and Z.-X. Hu, Biorthogonal Dynamical Quantum Phase Transitions in Non-Hermitian Systems, *Phys. Rev. Lett.* **132**, 220402 (2024).
- [57] Y. Ashida, Z. Gong, and M. Ueda, Non-Hermitian physics, *Adv. Phys.* **69**, 249 (2021).
- [58] C. W. Lv, R. Zhang, Z. Z. Zhai, and Qi Zhou, Curving the space by non-Hermiticity, *Nat. Commun.* **13**, 2184 (2022).
- [59] H. Jiang and C. H. Lee, Dimensional Transmutation from Non-Hermiticity, *Phys. Rev. Lett.* **131**, 076401 (2023).
- [60] P.-R. Han, F. Wu, X.-J. Huang, H.-Z. Wu, C.-L. Zou, W. Yi, M. Z. Zhang, H. K. Li, K. Xu, D. N. Zheng, H. Fan, J. M. Wen, Z.-B. Yang, and S.-B. Zheng, Exceptional Entanglement Phenomena: Non-Hermiticity Meeting Nonclassicality, *Phys. Rev. Lett.* **131**, 260201 (2023).
- [61] R. Sarkar, A. Bandyopadhyay, and A. Narayan, Non-Hermiticity induced exceptional points and skin effect in the Haldane model on a dice lattice, *Phys. Rev. B* **107**, 035403 (2023).
- [62] W. Y. Sun, L. Luo, Y. Y. Huang, J. B. Peng, D. G. Zhao, Y. W. Yao, F. G. Wu, and X. Zhang, Observation of acoustic hybrid-order topological insulator induced by non-Hermiticity and anisotropy, *Phys. Rev. B* **109**, 134302 (2024).
- [63] L. Xiao, Y. M. Chu, Q. Lin, H. Q. Lin, W. Yi, J. M. Cai, and P. Xue, Non-Hermitian Sensing in the Absence of Exceptional Points, *Phys. Rev. Lett.* **133**, 180801 (2024).
- [64] T. X. Dai, Y. T. Ao, J. Mao, Y. Yang, Y. Zheng, C. H. Zhai, Y. D. Li, J. Z. Yuan, B. Tang, Z. H. Li, J. Luo, W. W. Wang, X. Y. Hu, Q. H. Gong and J. W. Wang, Non-Hermitian topological phase transitions controlled by nonlinearity, *Nat. Phys.* **20**, 101 (2024).
- [65] X. Zhang, T. Zhang, M.-H. Lu, and Y.-F. Chen, A review on non-Hermitian skin effect, *Adv. Phys.: X* **7**, 2109431 (2022).
- [66] G.-G. Liu, S. Mandal, P. H. Zhou, X. Xi, R. Banerjee, Y.-H. Hu, M. G. Wei, M. R. Wang, Q. Wang, Z. Gao, H. S. Chen, Y. H. Yang, Y. D. Chong, and B. Zhang, Localization of Chiral Edge States by the Non-Hermitian Skin Effect, *Phys. Rev. Lett.* **132**, 113802 (2024).
- [67] J. Gliozzi, G. D. Tomasi, and T. L. Hughes, Many-Body Non-Hermitian Skin Effect for Multipoles, *Phys. Rev. Lett.* **133**, 136503 (2024).
- [68] T. Yoshida, S.-B. Zhang, T. Neupert, and N. Kawakami, Non-Hermitian Mott Skin Effect, *Phys. Rev. Lett.* **133**, 076502 (2024).
- [69] S. Wittrock, S. Perna, R. Lebrun, K. Ho, R. Dutra, R. Ferreira, P. Bortolotti, C. Serpico and V. Cros, Non-hermiticity in spintronics: oscillation death in coupled spintronic nano-oscillators through emerging exceptional points, *Nat. Commun.* **15**, 971 (2024).
- [70] C. Wang and X. R. Wang, Anderson localization transitions in disordered non-hermitian systems with exceptional points, *Phys. Rev. B* **107**, 024202 (2023).
- [71] V. M. Martinez Alvarez, J. E. Barrios Vargas, L. E. F. Foa Torres, Non-Hermitian robust edge states in one dimension: Anomalous localization and eigenspace condensation at exceptional points, *Phys. Rev. B* **97**, 121401(R) (2018).
- [72] A. Li, H. Wei, M. Cotrufo, W. Chen, S. Mann, X. Ni, B. Xu, J. Chen, J. Wang, S. Fan, C.-W. Qiu, A. Al, and L. Chen, Exceptional points and non-Hermitian photonics at the nanoscale, *Nat. Nanotechnol.* **18**, 706 (2023).
- [73] J. Wingenbach, S. Schumacher, and X. K. Ma, Manipulating spectral topology and exceptional points by nonlinearity in non-Hermitian polariton systems, *Phys. Rev. Research* **6**, 013148 (2024).
- [74] H. Jiang, L.-J. Lang, C. Yang, S.-L. Zhu, and S. Chen, Interplay of non-hermitian skin effects and Anderson localization in nonreciprocal quasiperiodic lattices, *Phys. Rev. B* **100**, 054301 (2019).
- [75] C.-X. Guo, C.-H. Liu, X.-M. Zhao, Y. Liu, and S. Chen, Exact solution of non-Hermitian systems with generalized boundary conditions: Size-dependent boundary effect and fragility of the skin effect, *Phys. Rev. Lett.* **127**, 116801 (2021).
- [76] A. P. Acharya and S. Datta, Localization transitions in a non-Hermitian quasiperiodic lattice, *Phys. Rev. B* **109**, 024203 (2024).
- [77] C.-X. Guo, L. H. Su, Y. L. Wang, L. Li, J. Z. Wang, X. H. Ruan, Y. J. Du, D. N. Zheng, S. Chen, and H. P. Hu, Scale-tailored localization and its observation in non-Hermitian electrical circuits, *Nat. Commun.* **15**, 9120 (2024).
- [78] D. Kochergin, V. Tiselko, and A. Onuchin, Localization transition in non-Hermitian systems depending on reciprocity and hopping asymmetry, *Phys. Rev. E* **109**, 044315 (2024).
- [79] L.-J. Zhai, S. Yin, and G.-Y. Huang, Many-body localization in a non-hermitian quasiperiodic system, *Phys. Rev. B* **102**, 064206 (2020).
- [80] N. Hatano and D. R. Nelson, Localization transitions in non-Hermitian quantum mechanics, *Phys. Rev. Lett.* **77**, 570 (1996).
- [81] N. Hatano and D. R. Nelson, Non-Hermitian delocalization and eigenfunctions, *Phys. Rev. B* **58**, 8384 (1998).
- [82] X.-W. Luo and C. Zhang, Photonic topological insulators induced by non-Hermitian disorders in a coupled-cavity array, *Appl. Phys. Lett.* **123**, 081111 (2023).

- [83] W. Chen, S. Cheng, J. Lin, R. Asgari, and X. Gao, Breakdown of the correspondence between the real-complex and delocalization-localization transitions in non-Hermitian quasicrystals, *Phys. Rev. B* **106**, 144208 (2022).
- [84] Z.-H. Wang, F. Xu, L. Li, D.-H. Xu, and B. Wang, Topological superconductors and exact mobility edges in non-Hermitian quasicrystals, *Phys. Rev. B* **105**, 024514 (2022).
- [85] S. Longhi, Non-Hermitian Maryland model, *Phys. Rev. B* **103**, 224206 (2021).
- [86] A. Jazaeri and I. I. Satija, Localization transition in incommensurate non-Hermitian systems, *Phys. Rev. E* **63**, 036222 (2001).
- [87] P. Wang, L. Jin, and Z. Song, Non-Hermitian phase transition and eigenstate localization induced by asymmetric coupling, *Phys. Rev. A* **99**, 062112 (2019).
- [88] L.-Z. Tang, G.-Q. Zhang, L.-F. Zhang, and D.-W. Zhang, Localization and topological transitions in non-Hermitian quasiperiodic lattices, *Phys. Rev. A* **103**, 033325 (2021).
- [89] C. Wu, J. Fan, G. Chen, and S. Jia, Non-Hermiticity-induced reentrant localization in a quasiperiodic lattice, *New J. Phys.* **23**, 123048 (2021).
- [90] R. Hamazaki, K. Kawabata, and M. Ueda, Non-Hermitian many-body localization, *Phys. Rev. Lett.* **123**, 090603 (2019).
- [91] L.-J. Zhai, G.-Y. Huang, and S. Yin, Nonequilibrium dynamics of the localization-delocalization transition in the non-Hermitian Aubry-André model, *Phys. Rev. B* **106**, 014204 (2022).
- [92] L.-J. Zhai, L.-L. Hou, Q. Gao, and H.-Y. Wang, Kibble-Zurek scaling of the dynamical localization-skin effect phase transition in a non-Hermitian quasi-periodic system under the open boundary condition, *Front. Phys.* **10**, 1098551 (2022).
- [93] Z. H. Xu and S. Chen, Dynamical evolution in a one-dimensional incommensurate lattice with PT symmetry, *Phys. Rev. A* **103**, 043325 (2021).
- [94] Y.-M. Sun, X.-Y. Wang and L.-J. Zhai, Hybrid scaling properties of the localization transition in a non-Hermitian disordered Aubry-André model, *Phys. Rev. B* **110**, 054202 (2024).
- [95] J. Bauer, T. M. Chang, and J. L. Skinner, Correlation length and inverse-participation-ratio exponents and multifractal structure for Anderson localization, *Phys. Rev. B* **42**, 8121 (1990).
- [96] Y. V. Fyodorov and A. D. Mirlin, Analytical derivation of the scaling law for the inverse participation ratio in quasi-one-dimensional disordered systems, *Phys. Rev. Lett.* **69**, 1093 (1992).
- [97] F. Zhong, Probing criticality with linearly varying external fields: Renormalization group theory of nonequilibrium critical dynamics under driving, *Phys. Rev. E* **73**, 047102 (2006).
- [98] S. Gong, F. Zhong, X. Huang, and S. Fan, Finite-time scaling via linear driving, *New J. Phys.* **12**, 043036 (2010).
- [99] Y. Huang, S. Yin, B. Feng, and F. Zhong, Kibble-Zurek mechanism and finite-time scaling, *Phys. Rev. B* **90**, 134108 (2014).
- [100] G. D. Tomasi and I. M. Khaymovich, Non-Hermiticity induces localization: Good and bad resonances in power-law random banded matrices, *Phys. Rev. B* **108**, L180202 (2023).
- [101] S. Longhi, Non-Hermitian control of localization in mosaic photonic lattices, *Appl. Phys. Lett.* **123**, 161102 (2023).